Research Article | Vol. 25, No. 7 | 3 Apr 2017 | OPTICS EXPRESS 8267
Optics EXPRESS

Diffractive *m*-bonacci lenses

FEDERICO MACHADO,[1] VICENTE FERRANDO,[2] WALTER D. FURLAN,[2] AND JUAN A. MONSORIU[1,*]

[1]*Centro de Tecnologías Físicas, Universitat Politècnica de València, 46022 Valencia, Spain*
[2]*Departamento de Óptica, Universitat de València, 46100 Burjassot, Spain*
**jmonsori@fis.upv.es*

Abstract: Fibonacci zone plates are proving to be promising candidates in image forming devices. In this letter we show that the set of Fibonacci zone plates are a particular member of a new family of diffractive lenses which can be designed on the basis of a given *m*-bonacci sequence. These lenses produce twin axial foci whose separation depends on the *m*-golden mean. Therefore, with this generalization, bifocal systems can be freely designed under the requirement at particular focal planes. Experimental results support our proposal.

OCIS codes: (050.0050) Diffraction and gratings; (050.1965) Diffractive lenses.

References and links

1. G. Saavedra, W. D. Furlan, and J. A. Monsoriu, "Fractal zone plates," Opt. Lett. **28**(12), 971–973 (2003).
2. J. A. Monsoriu, C. J. Zapata-Rodriguez, and W. D. Furlan, "Fractal axicons," Opt. Commun. **263**(1), 1–5 (2006).
3. Q. Zhang, J. Wang, M. Wang, J. Bu, S. Zhu, B. Z. Gao, and X. Yuan, "Depth of focus enhancement of a modified imaging quasi-fractal zone plate," Opt. Laser Technol. **44**(7), 2140–2144 (2012).
4. W. D. Furlan, G. Saavedra, and J. A. Monsoriu, "White-light imaging with fractal zone plates," Opt. Lett. **32**(15), 2109–2111 (2007).
5. V. Ferrando, F. Giménez, W. D. Furlan, and J. A. Monsoriu, "Bifractal focusing and imaging properties of Thue-Morse Zone Plates," Opt. Express **23**(15), 19846–19853 (2015).
6. F. Giménez, W. D. Furlan, A. Calatayud, and J. A. Monsoriu, "Multifractal zone plates," J. Opt. Soc. Am. A **27**(8), 1851–1855 (2010).
7. J. Monsoriu, G. Saavedra, and W. Furlan, "Fractal zone plates with variable lacunarity," Opt. Express **12**(18), 4227–4234 (2004).
8. H. Dai, J. Liu, S. Xuecheng, and Y. Dejin, "Programmable fractal zone plates (FraZPs) with foci finely tuned," Opt. Commun. **281**(22), 5515–5519 (2008).
9. R. Verma, M. K. Sharma, P. Senthilkumaran, and V. Banerjee, "Analysis of Fibonacci gratings and their diffraction patterns," J. Opt. Soc. Am. A **31**(7), 1473–1480 (2014).
10. F. Giménez, J. A. Monsoriu, W. D. Furlan, and A. Pons, "Fractal photon sieve," Opt. Express **14**(25), 11958–11963 (2006).
11. V. Ferrando, A. Calatayud, F. Giménez, W. D. Furlan, and J. A. Monsoriu, "Cantor dust zone plates," Opt. Express **21**(3), 2701–2706 (2013).
12. S. H. Tao, B. C. Yang, H. Xia, and W. X. Yu, "Tailorable three-dimensional distribution of laser foci based on customized fractal zone plates," Laser Phys. Lett. **10**(3), 035003 (2013).
13. A. Calabuig, S. Sánchez-Ruiz, L. Martínez-León, E. Tajahuerce, M. Fernández-Alonso, W. D. Furlan, J. A. Monsoriu, and A. Pons-Martí, "Generation of programmable 3D optical vortex structures through devil's vortex-lens arrays," Appl. Opt. **52**(23), 5822–5829 (2013).
14. J. Pu and P. H. Jones, "Devil's lens optical tweezers," Opt. Express **23**(7), 8190–8199 (2015).
15. S. Cheng, X. Zhang, W. Ma, and S. Tao, "Fractal zone plate beam based optical tweezers," Sci. Rep. **6**(1), 34492 (2016).
16. X. Ge, Z. Wang, K. Gao, D. Wang, Z. Wu, J. Chen, Z. Pan, K. Zhang, Y. Hong, P. Zhu, and Z. Wu, "Use of fractal zone plates for transmission X-ray microscopy," Anal. Bioanal. Chem. **404**(5), 1303–1309 (2012).
17. W. D. Furlan, V. Ferrando, J. A. Monsoriu, P. Zagrajek, E. Czerwińska, and M. Szustakowski, "3D printed diffractive terahertz lenses," Opt. Lett. **41**(8), 1748–1751 (2016).
18. J. F. Barrera, M. Tebaldi, D. Amaya, W. D. Furlan, J. A. Monsoriu, N. Bolognini, and R. Torroba, "Multiplexing of encrypted data using fractal masks," Opt. Lett. **37**(14), 2895–2897 (2012).
19. M. Tebaldi, W. D. Furlan, R. Torroba, and N. Bolognini, "Optical-data storage-readout technique based on fractal encrypting masks," Opt. Lett. **34**(3), 316–318 (2009).
20. A. K. Yadav, S. Vashisth, H. Singh, and K. Singh, "A phase-image watermarking scheme in gyrator domain using devil's vortex Fresnel lens as a phase mask," Opt. Commun. **344**, 172–180 (2015).
21. R. Verma, V. Banerjee, and P. Senthilkumaran, "Fractal signatures in the aperiodic Fibonacci grating," Opt. Lett. **39**(9), 2557–2560 (2014).

#285616 https://doi.org/10.1364/OE.25.008267
Journal © 2017 Received 25 Jan 2017; revised 11 Mar 2017; accepted 11 Mar 2017; published 30 Mar 2017

Optics EXPRESS

22. K. Wu and G. P. Wang, "Two-dimensional Fibonacci grating for far-field super-resolution imaging," Sci. Rep. **6**(1), 38651 (2016).
23. V. Ferrando, A. Calatayud, P. Andrés, R. Torroba, W. D. Furlan, and J. A. Monsoriu, "Imaging properties of Kinoform Fibonacci lenses," IEEE Photonics J. **6**(1), 6500106 (2014).
24. N. Gao, Y. Zhang, and C. Xie, "Circular Fibonacci gratings," Appl. Opt. **50**(31), G142–G148 (2011).
25. J. A. Monsoriu, A. Calatayud, L. Remón, W. D. Furlan, G. Saavedra, and P. Andrés, "Bifocal Fibonacci diffraction lenses," IEEE Photonics J. **5**(3), 3400106 (2013).
26. A. Calatayud, V. Ferrando, L. Remón, W. D. Furlan, and J. A. Monsoriu, "Twin axial vortices generated by Fibonacci lenses," Opt. Express **21**(8), 10234–10239 (2013).
27. J. Ke and J. Zhang, "Generalized Fibonacci photon sieves," Appl. Opt. **54**(24), 7278–7283 (2015).
28. T. Noe, T. Piezas, and E. W. Weisstein, "Fibonacci n-Step Number," From MathWorld–A Wolfram Web Resource. *http://mathworld.wolfram.com/Fibonaccin-StepNumber*.
29. J. A. Monsoriu, M. H. Giménez, W. D. Furlan, J. C. Barreiro, and G. Saavedra, "Diffraction by m-bonacci gratings," Eur. J. Phys. **36**(6), 65005 (2015).

1. Introduction

Photonics technology has benefited in recent years by the emergence of several novel devices designed and constructed using quasi-periodic and fractal structures. Diffractive Optical Elements (DOEs) designed with such structures have been demonstrated unique features with multiple applications [1–20]. Fractal zone plates (FZPs), introduced in 2003 by our group [1], are multifocal lenses that exhibit a wide depth of focus [2,3] and have low chromatic aberration [4–6]. It has been shown, that the focal length of a FZP can by finely tuned by means of the so-called *lacunarity* of the structure [7,8]. This feature in conjunction with the intrinsic self-similarity of the fractal beam produce, allow simultaneous optical trapping and manipulation of multiple particles, separately, at different focal planes [12,13]. Therefore, FZP beams would be useful for constructing versatile 3D optical tweezers [14,15]. FZPs have found applications in ranges of the electromagnetic spectrum outside of the visible. In a transmission X-ray microscope, FZP was proposed not only as an image-forming lens but also as a condenser element to achieve an extended depth of field [16]. Promising applications in THz technology were also recently proposed [17].

FZPs are also able to perform multiplexing of encrypted data [18,19] and their generalized blaze counterparts: the Devil's vortex lenses provide rich phase masks which contribute to enhance security (robustness against occlusion and noise attacks) in watermarking schemes in addition to overcoming the problem of axis alignment in the optical setup [20].

Among aperiodic based DOEs, Fibonacci gratings [9,21] have been used to transform evanescent waves into propagating waves for superresolution imaging. In addition, the selfsimilarity of these structures is important because render them robust against manufacturing defects and damages. It has been proved that DOEs with nearly 50% of degradation, can still be used in image-forming devices without loss of performance capabilities, allowing applications in harmful working conditions [22]. Fibonacci zone plates [23–27] stand out for producing two foci, that are located one in front and one behind the focus of an equivalent Fresnel zone plate of the same number of zones. The axial positions of these foci are given by the Fibonacci numbers, being the golden mean the ratio of the two focal distances. The golden mean also accounts for the energetic balance of both foci and for their axial and transverse resolution.

It is important to note that the above-mentioned aperiodic based DOEs do not have special requirements to be produced (i.e. not different from the equivalent Fresnel zone plates). Indeed, several methods have been employed to do that, like printing on graphic films using a high resolution photo-plotter [5], chemically amplified photoresist by UV laser direct writing technique [3], 3-D printing [17], and more frequently, using liquid crystal on silicon spatial light modulators (SLMs) [5,8,13–15,17].

In this work, we present the *m*-bonacci zone plates as a meaningful generalization of the Fibonacci zone plates. The focusing properties of this family of DOEs is investigated and the imaging properties are experimentally verified.

Optics EXPRESS

2. Lens design

The new family of aperiodic diffractive lenses that we propose is inspired in the most general mathematical set of the recognized Fibonacci numbers which are known as the *m*-bonacci numbers [28, 29]. These sets of elements $\{N_{m,j}\}$ are defined by *m* digits $N_{m,0}=0$, $N_{m,1}=1$, and $N_{m,j}=\sum_{i=1}^{j}N_{m,j-1}$ with $1<j<m$, and are obtained by the iterative rule $N_{m,S}=\sum_{i=1}^{m}N_{m,S-1}$ with $S\geq m$. For example, to obtain the Tribonacci numbers $(m=3)$, we define the seeds: $N_{3,0}=0$, $N_{3,1}=1$, and $N_{3,2}=1$. The following Tribonacci numbers for $S\geq 3$ are obtained as the sum of the preceding three ones, resulting in the sequence $N_{3,i}=\{0,1,1,2,4,7,13,24,44,81\ldots\}$.

In the same way, the generalized golden mean or golden ratio is defined as the limit of the ratio of two consecutive *m*-bonacci numbers:

$$\varphi_m=\lim_{S\to\infty}\left(\frac{N_{m,S}}{N_{m,S-1}}\right) \tag{1}$$

It is easy to demonstrate that the above limit results in the transcendental equation

$$(\varphi_m)^m-\sum_{i=1}^{m}(\varphi_m)^{m-i}=0 \tag{2}$$

The above equation for $m=2$ (Fibonacci) has the following solution $\varphi_2\simeq 1.618$, i.e, the well-known golden ratio. For $m=3$ (Tribonacci) and $m=4$ (Tetranacci), the corresponding *m*-golden ratio are $\varphi_3\simeq 1.839$ and $\varphi_4\simeq 1.927$, respectively.

Based on the *m*-bonacci numbers, a binary *m*-bonacci sequence can also be generated with *m* binary elements, $t_{m,0}=\{0\}$ $t_{m,1}=\{1\}$, and $t_{m,j}=\{t_{m,j-1}\ t_{m,j-2}\ldots\ t_{m,0}\}$ with $1<j<m$, and the successive elements of the sequence are obtained as the concatenation of the *m* previous ones, $t_{m,S}=\{t_{m,S-1}\ t_{m,S-2}\ldots\ t_{m,S-m}\}$ with $S\geq m$ [28]. For example, for the construction of the Tribonacci sequence $(m=3)$, we use the seeds $t_{3,0}=\{0\}$, $t_{3,1}=\{1\}$ and $t_{3,2}=\{1,0\}$. The corresponding successive elements are obtained as the concatenation rule $t_{3,S}=\{t_{3,S-1},t_{3,S-2},t_{3,S-3}\}$, thus $t_{3,3}=\{1010\}$, $t_{3,4}=\{1010101\}$, $t_{3,5}=\{1010101101010\}$, and so on. Therefore, the *m*-bonacci binary sequence developed up to an arbitrary level *S*, contains $N_{m,S}$ type-1 elements and $\sum_{i=1}^{m-1}N_{m,S-i}=N_{m,S+1}-N_{m,S}$ type-0 elements, being the limit of the ratio between both type of elements

$$\tau_m=\lim_{S\to\infty}\left(\frac{N_{m,S}}{N_{m,S+1}-N_{m,S}}\right)=\frac{1}{\varphi_m-1}. \tag{3}$$

Note, that the Fibonacci sequence, $\tau_2=1/(\varphi_2-1)=\varphi_2\simeq 1.618$. For the Tribonacci and Tetranacci sequences, $\tau_3=1/(\varphi_3-1)\simeq 1.191$ and $\tau_4=1/(\varphi_4-1)\simeq 1.078$, respectively.

In this work, our aim is to show how each of these sequences, developed up to a given value of S, can be used to design a zone plate (ZP). For example, as shown in Fig. 1, from the tribonacci sequence, $t_{3,5}=\{1010101101010\}$ we define the binary generating function $q_{3,5}(\zeta)$ with compact support on the interval [0, 1]. Since, like a conventional Fresnel ZP, a

Optics EXPRESS

m-bonacci ZP consists of a set of radially symmetric rings of the same area, the binary radial profile of the lens, *r*, can be obtained by performing the change of coordinates $\zeta = (r/a)^2$, where *a* is the external radius of the lens. The transmittance of the *l*-th ring is given by the value of the *l*-th element (1 or 0) of the *m*-bonacci sequence $t_{m,S}$.

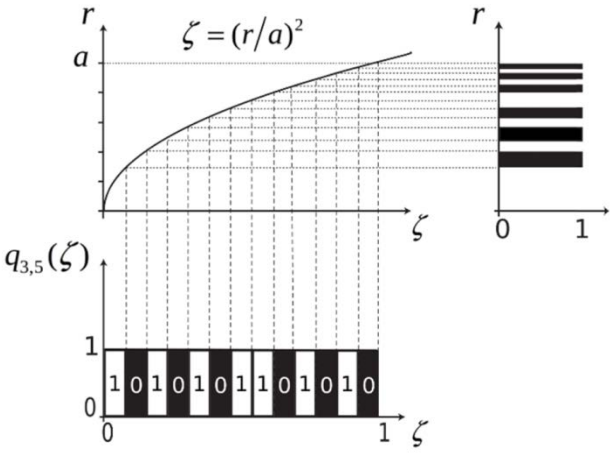

Fig. 1. Scheme for the construction of the radial profile of a tribonacci zone plate from the sequence $t_{3,5} = \{1010101101010\}$.

In general, the transmittance function, $q_{m,S}$, of a *m*-bonacci ZP of order S can be expressed as:

$$q_{m,S}(\zeta) = \sum_{l=1}^{N_{m,S+1}} t_{m,S,l}\ \mathrm{rect}(\zeta - l + 1/2), \tag{4}$$

3. Focusing properties

To evaluate the focusing properties of these new diffractive lenses we have computed the axial irradiance provided by them under monochromatic plane wave illumination of wavelength λ. Within the Fresnel approximation, the irradiance along the reduced axial coordinate $u = a^2/2\lambda z$ is given by

$$I(u) = 4\pi u^2 \left| \int_0^1 q(\zeta) exp(-i\,2\pi u\,\zeta) d\zeta \right|^2 \tag{5}$$

Two particular examples of m-bonacci lenses have been considered, both for the same level $S = 8$, the *tri*-bonacci and *tetra*-nacci zone plates: These lenses are shown in Fig. 2. By replacing corresponding the transmittance functions $q_{3,8}(\zeta)$ and $q_{4,8}(\zeta)$ in Eq. (5) we have numerically obtained the results shown in Fig. 3. It can be seen that the quasi-periodic distribution of zones according to the *m*-bonacci sequence produces a splitting of the focus (first diffraction order) in two irradiance peaks located at $u_a \simeq N_{3,8} = 44$ and $N_{3,9} - N_{3,8} = 81 - 44 = 37$, for the Tribonacci ZP; and at $u_a \simeq N_{4,8} = 56$ and $u_b \simeq N_{4,9} - N_{4,8} = 108 - 56 = 52$, for the Tetranacci ZP. Thus, interestingly, the ratio of the transverse distances for both lenses satisfies $u_a / u_b \simeq \tau_m = 1/(\varphi_m - 1)$. In fact, we have verified that, this result holds in general for every *m*-bonacci ZP. Moreover, we have also verified that this property is satisfied by *m*-bonacci ZP where the transparent and opaque

Optics EXPRESS

zones have different area. In all these cases, the position of the two foci also tends to $u_a \simeq N_{m,S}$ and $u_b \simeq N_{m,S+1} - N_{m,S}$, but its relative maxima depend on the zones width.

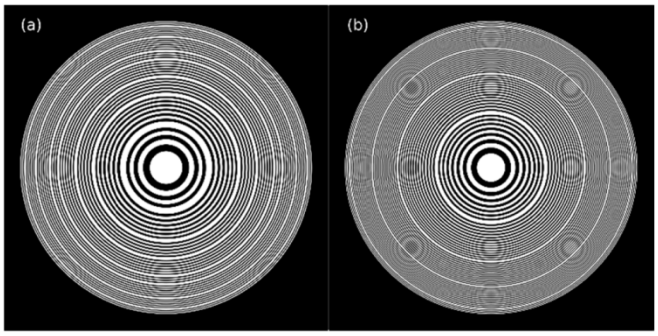

Fig. 2. a) Diffractive Tribonacci $(m = 3)$ and (b) Tetranacci $(m = 4)$ lenses designed for $S = 8$. The number of zones in (a) and (b) are $N_{3,8} = 81$ and $N_{4,8} = 108$, respectively.

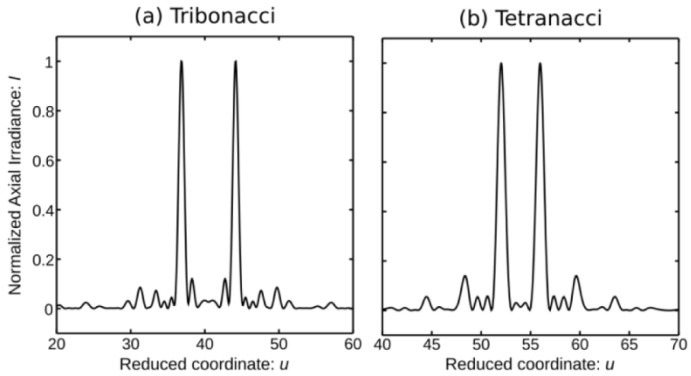

Fig. 3. Normalized axial irradiance versus the normalized reduced axial coordinate produced by the (a) diffractive Tribonacci and (b) Tetranacci lenses shown in Fig. 2.

4. Imaging properties

To test the image forming capabilities of *m*-bonacci ZPs we have employed the experimental setup shown in Fig. 4. The *m*-bonacci ZPs shown in Fig. 2 were implemented on a Liquid Crystal in a Silicon SLM (Holoeye PLUTO, 8-bit gray-level, pixel size 8 μm, and resolution 1920 × 1080 pixels), calibrated for 632.8 nm wavelength. The illumination system consisted of a collimated LED (Mounted High-Power LED, CW, 1000 mA). A filter allows us to select a wavelength in the visible range λ = 633 nm with a bandwidth of 10 nm. The beam was collimated by the lens L1 (focal length 100 mm) and directed to a test object (a smiley face), which was located at the focal plane of the lens L2 (focal length 200 mm). In addition to each *m*-bonacci lens, a linear phase carrier was modulated on the SLM to drive the light diffracted by of the odd zones of the lens out of the optical axis, generating in this way the dark zones of the amplitude lens and to avoid noise originating from the specular reflection (zero order of diffraction). This linear phase is compensated by tilting the SLM. In this way, the addressed signal was guided by the first diffraction order into the focal plane of lens L3 where a diaphragm (D) filters all diffraction orders except the first one. Lenses L3 (focal length 200 mm) and L4 (focal length 100 mm) conform a 4*f* setup with 0.5 magnification. Then at the L4 lens focal plane (exit pupil) a rescaled image of the desired lens pupil is achieved. Images of the test object produced by the diffractive lenses were then captured and registered with a CCD camera (8 bit gray-level, pixel pitch of 3.75 μm, and 1280 × 960 pixels) mounted on a

Optics EXPRESS

translation stage (Thorlabs LTS 300; range 300 mm; precision 5 μm) along the optical axis (z).

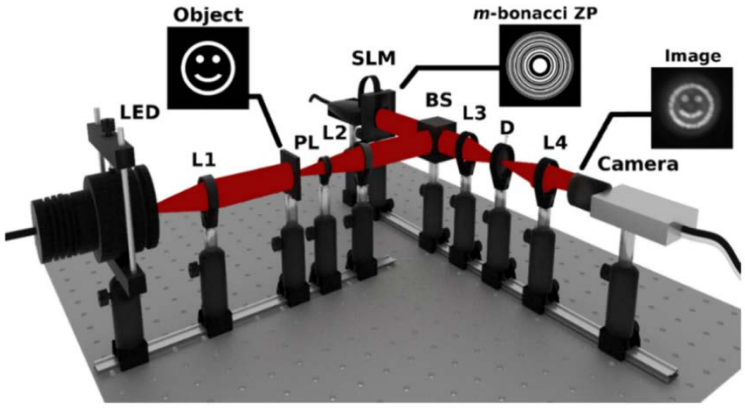

Fig. 4. Experimental setup. L1 and L4 are 100 mm focal distance lenses. L2 and L3 are 200 mm focal distance lenses. BS is a beam splitter, D is an iris diaphragm, and PL a linear polarizer. The translation stage shifts the camera in order to get images along z-axis (see the main text for details).

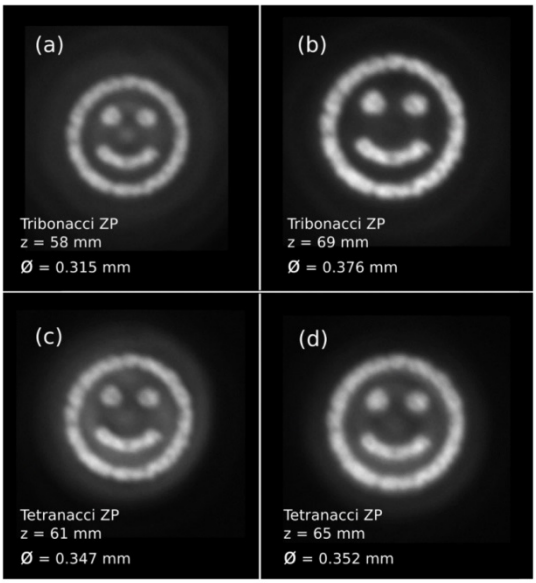

Fig. 5. Twin images obtained with the m-bonacci lenses shown in Fig. 2.

The registered images obtained at each focal plane of a Tribonacci lens with $a = 1.8$ mm and a Tetranacci lens with $a = 2.078$ mm are shown in Fig. 5. The experimental results were reproduced without any post-processing. Note that the ratios between the image plane distances agree with the relationship $u_a / u_b = z_b / z_a \simeq \tau_m$. In fact, distances in Fig. 5 (a) (Tribonacci) are $z_a = 58$ mm and $z_b = 69$ mm, and their ratio: $z_b / z_a = 1.189$, which is in good agreement with the theoretical value $\tau_3 \simeq 1.191$ (see Fig. 3). For the Tetranacci case, we obtained $z_c = 61$ mm and $z_d = 65$ mm and $z_d / z_c = 1.066$. Again, this result is well matched by the predicted value $\tau_4 \simeq 1.078$. On the other hand, it can be observed that relative diameter Ø of the images at both focal planes are also related by the m-golden ratio. In fact, if we

Optics EXPRESS

divide for each lens the diameter of the images shown in Fig. 5, we obtain approximately τ_m . In Fig. 5 the resolution of the lenses is limited by the width of the outermost ring (as happens for a Fresnel zone plate). Therefore, the tribonacci lens has a lower resolution than the Tetranacci lens. On the other hand, as there are two axial foci, the images corresponding to each focus have a reduced contrast because the twin out-of-focus image is superimposed to the in-focus image. This effect is more evident when both images become closer as happens for the Tetranacci images compared with Tribonacci ones.

5. Conclusions

We have presented a new family of diffractive lenses based on the generalized *m*-bonacci sequence. These lenses are naturally bifocals and the ratio of the two focal distances is related with the *m*-golden mean involved in the quasi-periodic structure. The imaging capabilities of the tribonacci and tetranacci lenses have been demonstrated experimentally. As the axial separation between the two foci can be tuned by a proper selection of the *m*-order, and taking into account that at present there are electronic devices that can be switchable at near real time to allow different configurations, these lenses offer a versatile alternative that can be advantageously used in several potential applications as for instance, bifocal contact and intraocular lenses, multiple plane optical trapping, optical micromachining, and confocal microscopy. Additionally, the concept of *m*-bonacci lenses can be easily extended to other geometries, like compound zone plates [6], photon sieves [10] and square zone plates [11].

Funding

This work was supported by the Ministerio de Economía y Competitividad and FEDER (Grant DPI2015-71256-R) and by the Generalitat Valenciana (Grant PROMETEOII-2014-072), Spain.

Acknowledgment

F. Machado also acknowledges a fellowship of MayaNet - Erasmus Mundus, Partnership 552061-EM-1-2014-1-IT-ERA MUNDUS-EMA21 (14-0872/001-001).